Fall 11-15-2016

Fabrication of High Performing Pemfc Catalyst-Coated Membranes with a Low Cost Air-Assisted Cylindrical Liquid Jets Spraying System

Xiong Peng

Travis Omasta

William Rigdon

William E. Mustain
University of South Carolina - Columbia, mustainw@mailbox.sc.edu

Publication Info

Published in *Journal of Electrochemical Society*, Volume 164, Issue 14, Fall 2016, pages E407-E413.

Fall 11-15-2016

Fabrication of High Performing PEMFC Catalyst-Coated Membranes with a Low Cost Air-Assisted Cylindrical Liquid Jets Spraying System

Mustain E William
University of South Carolina - Columbia, mustainw@mailbox.sc.edu

Publication Info

Published in *Journal of Electrochemical Society*, Volume 164, Issue 14, Fall 2016, pages E407-E413.

William E, Mustain (2016). Fabrication of High Performing PEMFC Catalyst-Coated Membranes with a Low Cost Air-Assisted Cylindrical Liquid Jets Spraying System. Journal of The Electrochemical Society, 163(14), E407-E413.
https://dx.doi.org/10.1149/2.0981614jes

Fabrication of High Performing PEMFC Catalyst-Coated Membranes with a Low Cost Air-Assisted Cylindrical Liquid Jets Spraying System

Xiong Peng, Travis Omasta,* William Rigdon, and William E. Mustain**,z**

Department of Chemical and Biomolecular Engineering, University of Connecticut, Storrs, Connecticut 06269, USA

In this work, a low cost air-assisted cylindrical liquid jets spraying (ACLJS) system was developed to prepare high-performance catalyst-coated membranes (CCMs) for proton exchange membrane fuel cells (PEMFCs). The catalyst ink was flowed from a cylindrical orifice and was atomized by an air stream fed from a coaxial slit and sprayed directly onto the membrane, which was suctioned to a heated aluminum vacuum plate. The CCM pore architecture including size, distribution and volume can be controlled using various flow parameters, and the impact of spraying conditions on electrode structure and PEMFC performance was investigated. CCMs fabricated in the fiber-type break-up regime by ACLJS achieved very high performance during PEMFC testing, with the top-performing cells having a current density greater than 1900 mA/cm^2 at 0.7 V under H_2/O_2 flows and 700 mA/cm^2 under H_2/Air at 1.5 bar$_{(absolute)}$ pressure and 60% gas RH, and 80°C cell temperature.

Manuscript submitted September 20, 2016; revised manuscript received November 7, 2016. Published November 15, 2016.

PEMFCs have long been considered to be among the most promising next-generation energy conversion systems for portable devices and transportation vehicles due to their zero or low pollution, high power density and low temperature operation.[1–3] However, the widespread commercialization of PEMFCs remains challenged by the high cost of cell assembly and the requirement of durable performance. In the last decade, significant efforts have been launched to make the technology cost competitive and to improve the cell performance by developing new electrocatalysts and lowering the noble metal loading.[4,5] However, the catalyst composition is not the only factor to consider when creating high-performance, low cost PEMFC electrodes.

The electrode pore structure plays a critical role in determining PEMFC performance, and it is a direct result of the application method. The electrode porosity and pore size distribution impact reaction kinetics and mass-transport processes, including water management and electron/proton conduction.[6–8] Structural optimization can be decisive in reducing performance losses, particularly at low catalyst loading and high current density.[9] In general, the catalyst coated membrane (CCM) method has been found to be superior to the gas diffusion layer (GDL) coating process because CCM fabrication avoids catalyst particles penetrating into the pore network of the GDL, lowering resistance at the interface with the electrolyte. For the CCM method, the catalyst ink can be applied onto the polymer membrane by brushing, screen printing, spraying, reactive spray deposition as well as roll-to-roll methods.[6,10–14] Among them, spraying has been commonly employed for CCM fabrication.[11,15,16] However, the effects of spraying conditions on the electrode structure and PEMFC performance are poorly understood in many systems, including the air-assisted cylindrical liquid jets spraying (ACLJS) system.

The objective of this work is to investigate the influence of spraying parameters on CCM structure and performance, with a particular focus on the ACLJS system because of its ability to produce very high performance CCMs at low initial capital cost, particularly at the lab scale. In the ACLJS system, colloidal ink is stripped from a nozzle by a high-speed annular gas flow, resulting in ink atomization. There are three distinct atomization regimes: Rayleigh-type breakup, membrane-type breakup and fiber-type breakup for coaxial air-liquid jets.[17] In this study, typical breakups of liquid were controlled by adjusting flow velocities of the gas and colloidal ink, and CCMs were prepared under all three atomization regimes: CCM-Ra, CCM-Me, and CCM-Fi for the Rayleigh-type breakup, membrane-type breakup and fiber-type breakup, respectively. The CCMs were analyzed by scanning electron microscopy (SEM) to assess surface morphology, as well as cross-section thickness and porosity. The CCM pore-size distributions were determined by mercury-intrusion porosimetry. The performance of these CCMs was tested in 25 cm^2 PEMFCs with standard protocols and their resistance during PEMFC testing was studied by electrochemical impedance spectroscopy (EIS).

Experimental

Materials and catalyst layer deposition.—The following is the recipe for a typical Pt/C ink preparation. First, a solvent mixture was prepared by adding 5.5 g of isopropanol to 3 g of 18.2 MOhm · cm DI water in a 10 mL Teflon vial, followed by a 5 min sonication. Next, 30 mg Pt/C (50 wt%, BASF) catalyst was added to a secondary 10 mL Teflon vial. The mixed solvent was transferred to the catalyst vial drop-by-drop by using a pipette, after which the mixture was sonicated for 10 min. Then, 180 mg of 5 wt% DE520 Nafion ionomer solution was added. The Teflon vial containing the catalyst ink was then transferred to an ultrasonicator (Fisher FS60) and sonicated for at least 60 min in an ice bath.

Schematics and pictures of the ACLJS are shown in Figures 1a–1d. The catalyst ink was dispensed from a syringe using a NE-1000 programmable syringe pump at a controlled rate, which then traversed through a Teflon tube (black line in Figure 1a) into the cylindrical jet, which was fed by a nitrogen cylinder. The liquid ink is mobilized by the fast-moving nitrogen gas stream when exiting the liquid flow nozzle, helping to form a wide distribution of fragment sizes.[18] The fragment structure of the ink carried from the nozzle to the substrate was set by the flow rates of the ink and carrier gas. The flow rates directly impact several dimensionless transport parameters, which are detailed in the supporting information, Equations S1-S6.[19] The type of ink breakup during transport from the nozzle to the substrate is typically controlled by the Weber number; We_R: Rayleigh-type breakup ($15 < We_R < 25$), membrane-type breakup ($25 < We_R < 70$) and fiber-type breakup ($100 < We_R < 500$).[17] The gas velocity and related dimensionless numbers are shown in Table S1 (supporting information). The microporous electrode architecture is formed when the atomized liquid fragments experience a sudden evaporation as they approach the heated substrate and make contact with the membrane. Such architecture helps water back diffusion and fuel mass transfer during fuel cell operation.[7,8]

The jet nozzle is moveable in two perpendicular directions that are parallel to the substrate surface, which is controlled by an

*Electrochemical Society Student Member.
**Electrochemical Society Member.
zE-mail: mustain@engr.uconn.edu

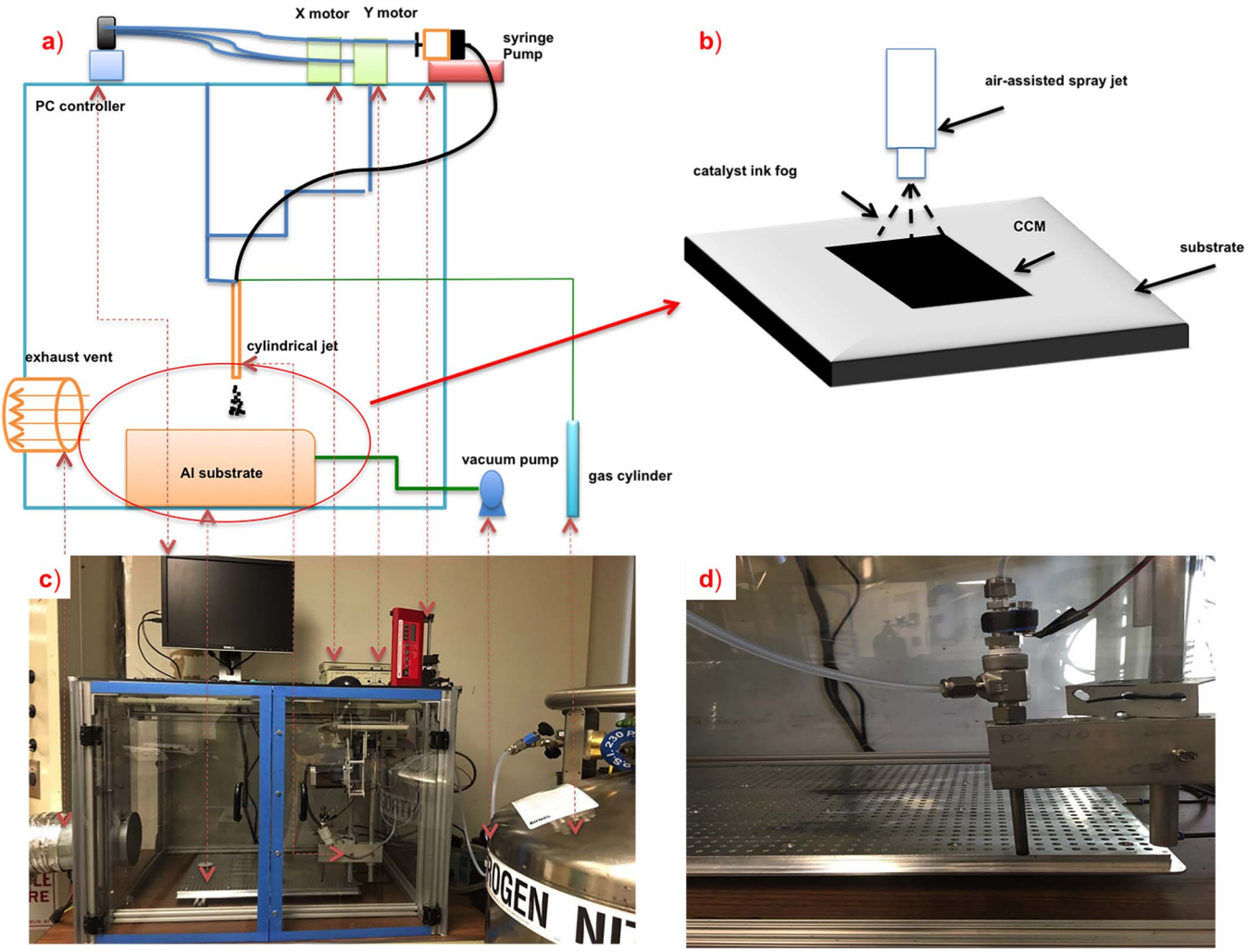

Figure 1. Air-assisted cylindrical liquid jet spraying system.

independent motor, enabling the fabrication of a uniform film (Figure S1a). By simply changing the moving distance of the nozzle in both perpendicular directions, a much larger active area CCM can be sprayed – up to 600 cm^2 – in this reported configuration. The spraying pattern, shown in Figure S1b, was controlled with a MD2xp Motor Control System, which enabled the independent movement of the nozzle in the x and y directions. All of the main components and their estimated costs are listed in Table S2. The CCM substrate, a Nafion-212 membrane, was fixed by a vacuum pump onto the heated aluminum substrate with a temperature of 80°C, which helped to avoid swelling and deformation of the Nafion membrane in the presence of the liquid isopropanol and water in the ink. The ACJLS system allows for precisely controlled electrode deposition thickness, which is essential to developing low electrocatalyst loading PEMFCs.[20]

Physical characterization.—The CCM surface morphology and cross-section were imaged using a FEI Quanta FEG 250 scanning electron microscope (SEM). The cross sections were prepared by rapid fracture after exposure to liquid nitrogen. Energy-dispersive X-ray spectroscopy (EDS) (TEAM EDS Analysis System) was used to estimate the elemental distribution in the CCM. The pore size distribution of the CCMs were determined by mercury intrusion porosimetry using a Micromeritics AutoPore IV 9500.

CCM testing in operating PEMFCs.—The CCMs were loaded into fuel cell hardware with 25 cm^2 active area, triple-pass serpentine flow fields on the cathode side and double-pass serpentine flow fields on the anode side. Sigracet 25 BC was used as the GDL. The average thickness of the CCM was 60 μm, the total thickness of the Teflon gaskets was 305 μm, and the total GDL thickness was 470 μm, which led to a pinch of 175 μm, corresponding to ∼33% of the total MEA thickness. The cell was humidified for three hours with H_2/N_2 at 0.2 L/min for the anode and cathode side at ambient pressure and activated overnight at 0.55 *V* with H_2/O_2 fed to the cell at anode and cathode stoichiometries of 2. The cell performance was tested with a Scribner 850e fuel cell test station. The performance was tested under H_2/O_2 flow with stoichiometry of 2 and also under H_2/Air flow with stoichiometry of 1.5/2 and a gas pressure of 150 $kPa_{(absolute)}$ on both sides. The cell temperature was 80°C and the anode and cathode dew points were 75°C and 73°C, respectively (81%/75% relative humidity).

Electrochemical impedance spectroscopy (EIS).—The cell impedance was determined using a Scribner Associates Model 890B unit with a Solartron Frequency Analyzer at three different current densities, 0.05, 0.5 and 1.5 A/cm^2, representing the kinetic, ohmic and mass transport regions of a PEMFC polarization curve. The EIS frequency range was 10 kHz–0.1 Hz. The impedance was measured in a galvanostatic mode by applying an AC current perturbation to the cell and measuring its voltage response. The amplitude of the AC current was constantly maintained at 5% of the DC current.

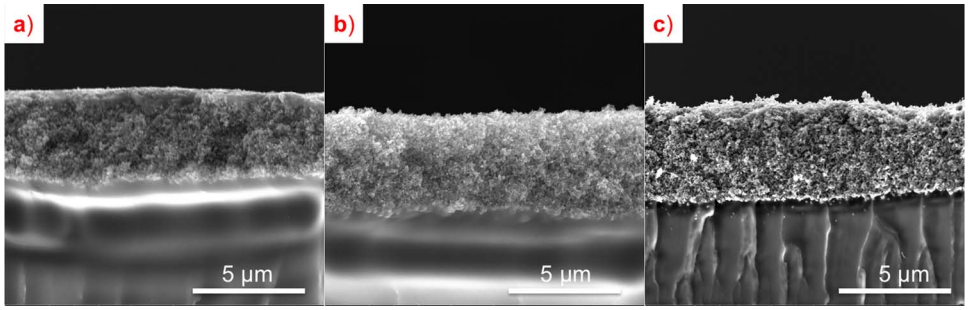

Figure 2. SEM cross-sections of (a) CCM-Ra; (b) CCM-Me and (c) CCM-Fi.

Results and Discussion

Physical characterization.—Cross-section micrographs for CCMs produced with all three types of ink breakup are shown in Figure 2. All catalyst layers (CLs) were well adhered to the Nafion 212 membrane, which helped reduce contact resistance. Droplet diameters that vary in orders of magnitude are produced in the three different types of breakup. In Rayleigh-type breakup, liquid drops are produced with diameter of the order of the jet diameter, while in membrane-type breakup, thin liquid sheets are developed that break into droplets of much smaller diameter than in Rayleigh-type breakup.[17] In fiber-type breakup, thin liquid fibers that peel off the jet are formed and break into ligaments downstream, which results in a complete atomization of the liquid ink.[17] As the ink becomes more atomized, the liquid ligaments evaporate faster than liquid drops with larger diameter when contacting the proton exchange membrane on the heated aluminum substrate, leading to faster phase separation of the solvent (IPA and water) and solid CL (catalyst and ionomer), which is beneficial for pore formation.

Therefore, driven by smaller droplet size and rapid solvent evaporation, CCM-Fi and CCM-Me showed a more porous structure and slight increase in average thickness than CCM-Ra due to higher total pore volume. This is shown both in the cross-section images of the CCMs in Figure 2 and surface images in Figure S2. In Figure S2, the images at lower magnification show the increased macro and meso porosity for CCM-Fi compared with CCM-Me and CCM-Ra. At higher magnification, CCM-Ra appears to be the densest while and CCM-Fi and CCM-Me look similar. Combining the SEM information at both magnifications, it appears that CCM-Fi should have the most meso and micro porosity, correlating well with the mercury intrusion porosimetry results shown below. All CCMs had enough large pores to allow for continuous supply of reactants. CCM-Ra showed a more dense surface than CCM-Me and CCM-Fi, indicating a shorter distance between carbon agglomerates, which led to a larger mass transport resistance and more difficult water management.

Previous studies suggested that a bimodal pore size distribution with primary pores (3–10 nm) inside agglomerates and secondary pores (10–50 nm) between agglomerates in the mesoporous region are able to maximize gas reactant as well as proton and water transport.[21,22] CCMs prepared by ACLJS also presented a bimodal pore size distribution (Figure 3a).

The CL architecture is supported mainly by carbon. The carbon particles tend to agglomerate in the colloidal ink if they are able to make contact with each other, which inhibits the formation of a bimodal pore structure if the deposition ink is not fully atomized. Because of this effect, CCM-Fi showed a wider distribution (3–10 nm) than CCM-Me and CCM-Ra (5–10 nm) and also a larger primary pore peak. CCM-Fi had extended secondary pores (10–100 nm) and a greater number of pores than CCM-Me and CCM-Ra in this range, which was due to improved atomization of catalyst ink during the spraying process. Therefore, CCM-Fi had a higher total pore volume than both CCM-Ra and CCM-Me, Figure 3b. CCM-Ra had lower pore volume relative to CCM-Me and CCM-Fi, which correlated well with the denser structure observed in Figure S2 caused by reduced distance between carbon agglomerates. Therefore, the microporous architecture of a CCM is a strong function of the ACLJS parameters, and it possible that the parameters can be tailored for a wide range of catalysts and substrates in order to achieve structures that are beneficial for mass transfer, increase the cell electrochemically active surface area and reduce electrode flooding.

SEM images of the cathode CL surface and cross-section of a CCM produced in the Fiber-type breakup regime are shown in Figures 4a–4d. Platinum nanoparticles appeared as bright dots and were distributed evenly throughout the CLs (Figure 4a), which is good for the formation of the triple-phase boundary.[10] The CL exhibited a very porous architecture and homogeneous agglomeration of carbon

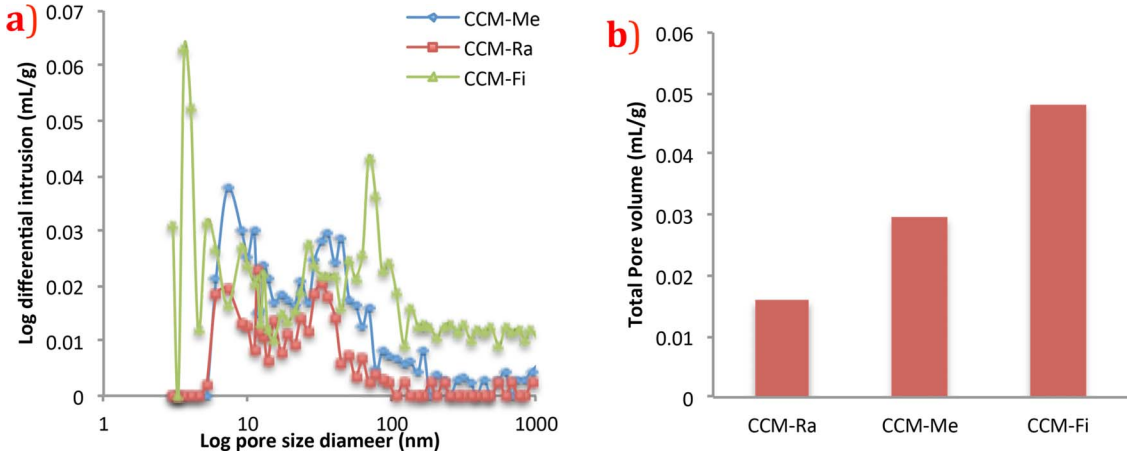

Figure 3. (a) Specific pore size distribution for CCM-Ra, CCM-Me and CCM-Fi; (b) Total pore volume for CCM-Ra, CCM-Me and CCM-Fi.

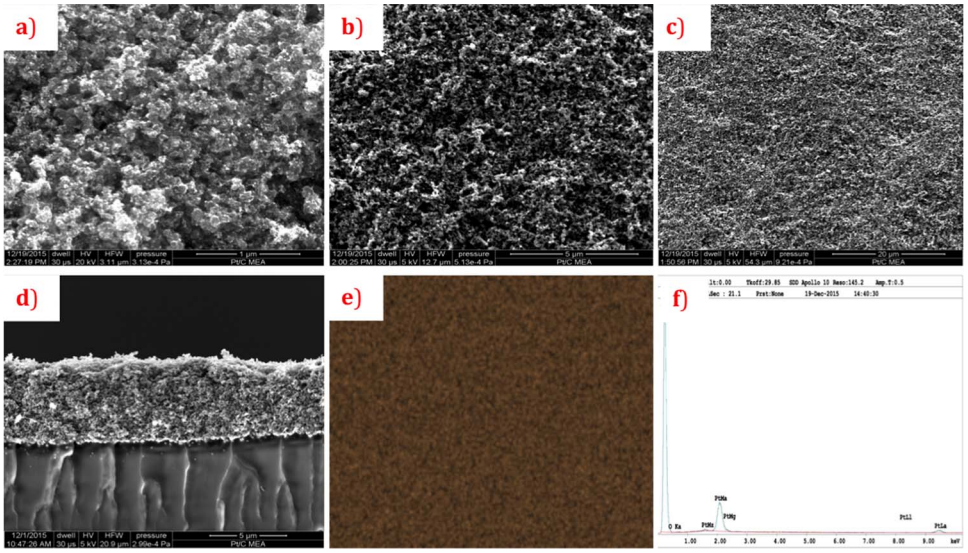

Figure 4. (a)-(d) surface and cross-section images of Pt/C CCMs prepared by air-assisted cylindrical liquid jet spraying system; (e) Pt elemental-mapping of the CL surface; (f) EDS spectra of Pt in the CL surface.

particles (Figures 4b and 4c) and did not show obvious cracks or mud-like morphologies that have been typically observed in previous CCM fabrication methods such as decal transfer and screen printing.[23,24] The CL had a thickness of around 5 micrometers (Figure 4d) after 81 passes, which took approximately 30 min. The CL surface was also characterized by EDS and elemental mapping (Figures 4e and 4f), from which the platinum showed a uniform distribution throughout the entirety of the studied area.

PEMFC performance and EIS study.—At least 3 CCMs of each flow type were prepared, and the results in all cases were reproducible-both in terms of fuel cell performance and pore structure obtained by mercury intrusion porosimetry. To simplify the data presentation, representative results for a single CCM each flow regime is presented. Figure 5a shows the H_2/O_2 polarization curves of the CCMs prepared at different conditions by the ACLJS system. All of the CCMs had approximately the same catalyst loading (0.3 ± 0.01 mg_{Pt}/cm^2) with the same ionomer to carbon ratio (3:5). The ORR kinetic region is shown in the inset of Figure 5a. CCM-Fi had the best observed ORR kinetics probably due to improved formation of the triple-phase boundary during CCM fabrication, which also corresponded to the lowest R_{ct} compared with the other two CCMs (Figure 6). In the H_2/O_2 polarization curves, the slope at intermediate and high current densities remained constant, indicating no significant mass transport loss within the measured current ranges. Additionally, non iR-corrected polarization data (Figure S3) showed that in the ohmic region of the polarization curve, the slope was smaller for CCM-Fi than CCM-Me and CCM-Ra, implying a lower ohmic resistance. When air was applied at the cathode (Figure 5b), mass transport became a very important distinguishing factor, particularly at high current densities. CCM-Fi showed by far the best performance compared with the other two CCMs when the cell was operated in H_2/Air, indicating that PEMFC performance can be efficiently improved at high current density by building a porous CL without increasing Pt loading.

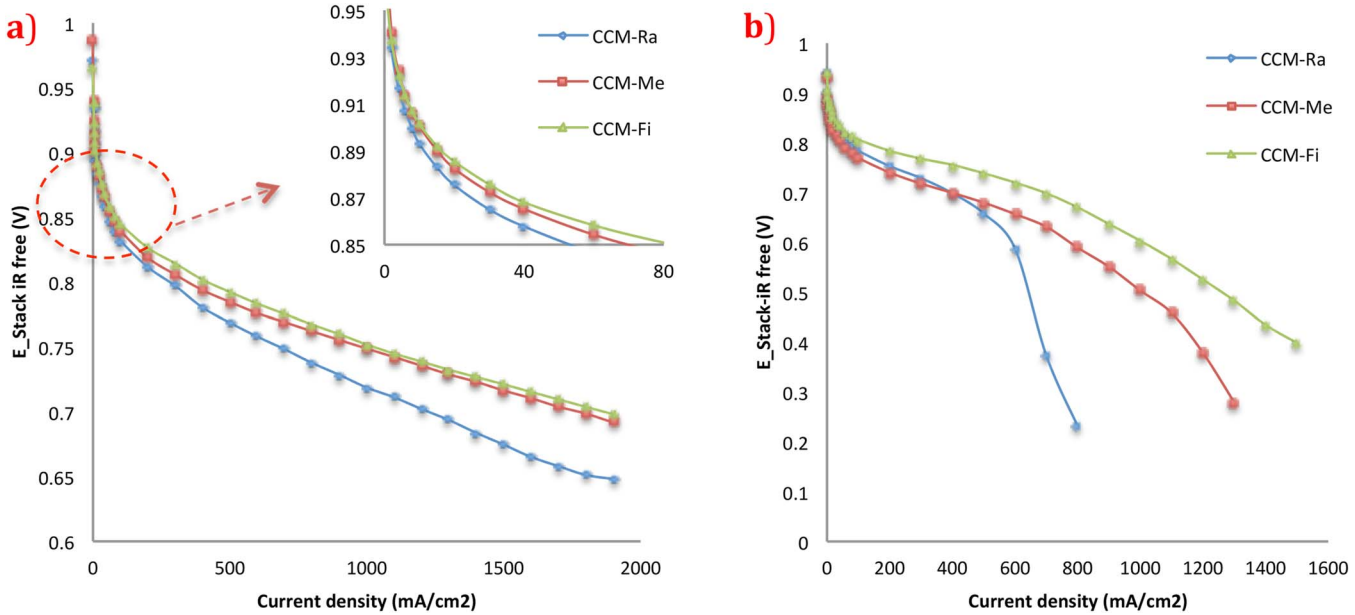

Figure 5. PEMFC performance of three CCMs at 80°C, 150 Kpa operating with (a) H_2/O_2 (b) H_2/Air flows.

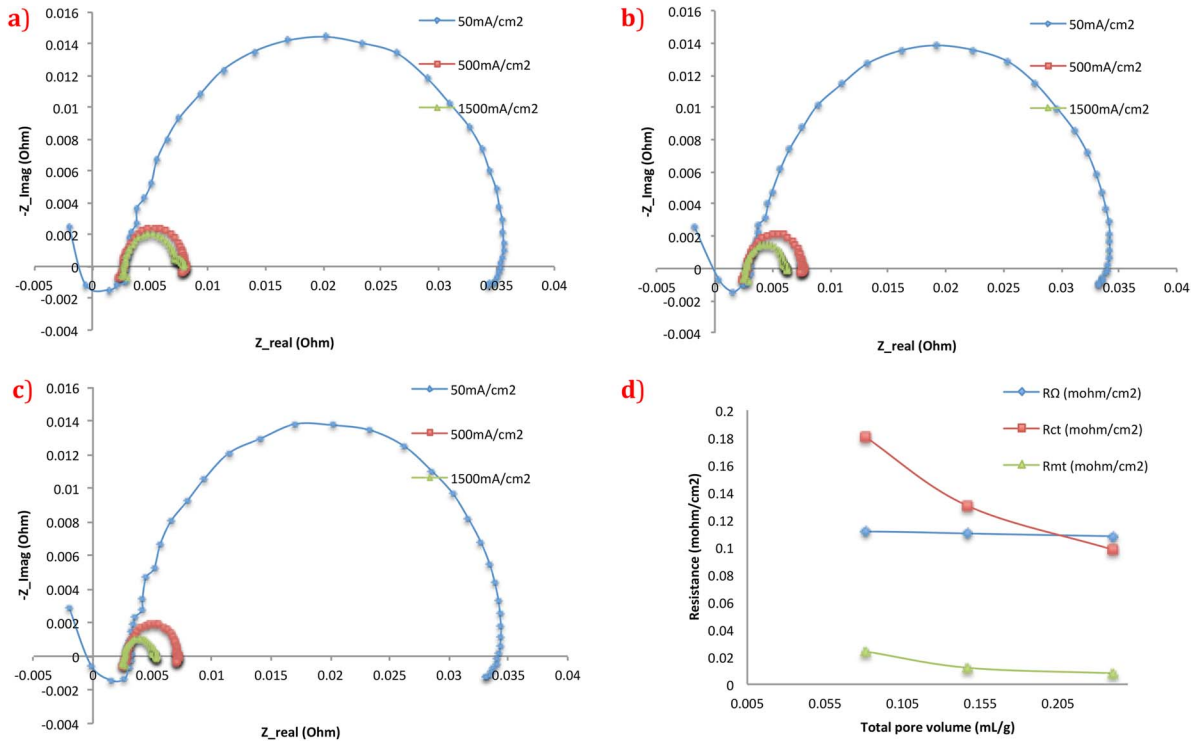

Figure 6. The AC impedance spectra at three current densities: 50 mA/cm^2, 500 mA/cm^2 and 1500 mA/cm^2 for (a) CCM-Ra; (b) CCM-Me; (c) CCM-Fi; (d) plot of resistances against total pore volume (resistance data is chosen from impedance spectra at 1500 mA/cm^2).

Nyquist plots for PEMFCs with the three CCM types at three typical current densities are shown in Figures 6a–6c. Pure hydrogen was fed to the anode to minimize anode polarization and the anode impedance was neglected in the analysis.[25] The equivalent circuits used to interpret the impedance results at low and high current density are shown in Figure S4.[26,27] The Nyquist plot at 50 mA/cm^2 was a single semicircle loop, indicating that the oxygen reduction reaction kinetics dominated the electrode behavior at this current density.[25] At higher current densities, a distortion of the kinetic loop was observed, resulting in two semicircles. The intermediate frequency semicircle represents the kinetic charge transfer resistance (R_{ct}) due to the oxygen reduction reaction within the CL[28] and the arc observed at low frequency represents the mass transport resistance (R_{mt}). The total ohmic resistance (R_Ω) was determined by the EIS high frequency intercept, which is comprised of the contact resistance and ohmic resistance in the cell components.[29]

In all cases, the charge transfer arc decreased while the mass transfer resistance increased as the current density was increased from

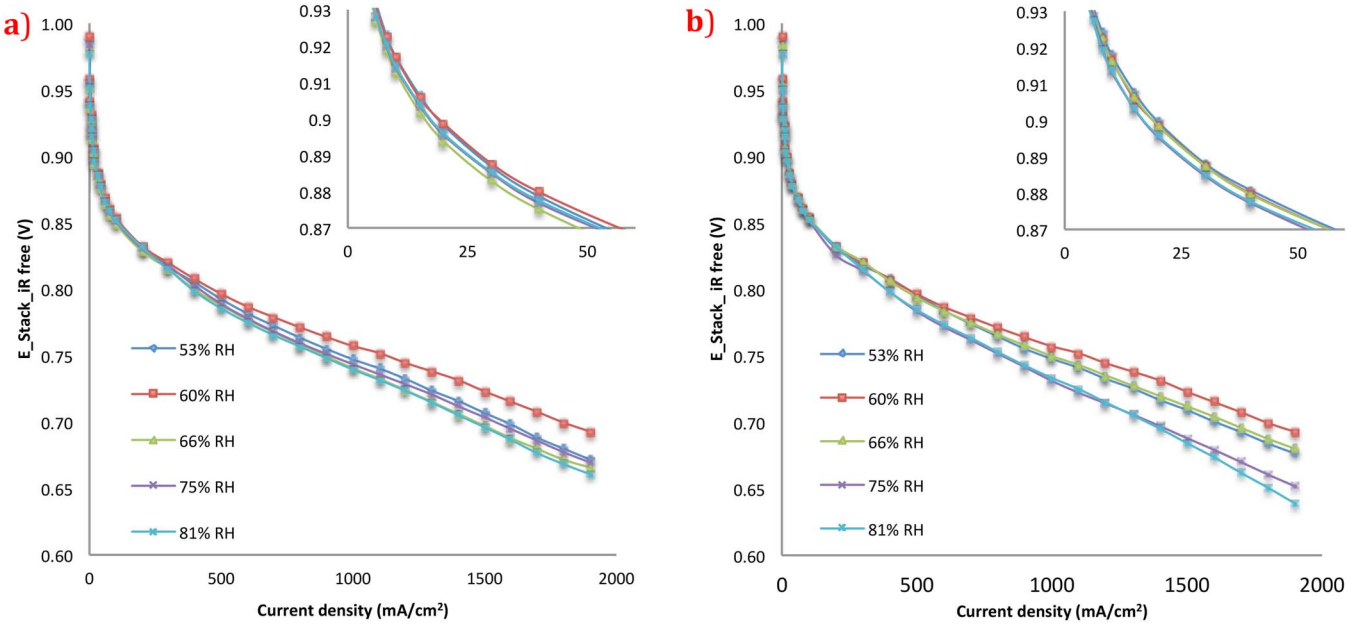

Figure 7. (a) Performance versus cathode relative humidity with constant 60% anode relative humidity; (b) Performance versus anode relative humidity with constant 60% cathode relative humidity.

500 mA/cm^2 to 1500 mA/cm^2, which showed the transition from kinetic to mass transport control. As the total pore volume increased from 0.08 mL/g to 0.24 mL/g, R_Ω experienced a slight decrease while R_{mt} and R_{ct} decreased by 66.7% and 45.6%, respectively (Figure 6d). The primary reason for this behavior is that a more porous CL helped to reduce the resistance for H_2/O_2 to diffuse to reaction sites and also reduce the resistance for the produced H_2O to move away from the CL. Increased CL porosity also decreases the impact of flooding in the CL on gas transfer and proton mobility and thus lowers both R_{mt} and R_{ct}. Therefore, CCM-Fi showed the highest performance because the fiber-type breakup yielded the highest total pore volume, which increases the contact area of gas reactants to active sites and thus increases current density at the same cell voltage. CCM-Fi also possessed an extended bimodal pore size distribution, which reduced mass transfer resistance and electrode flooding. The CCM-Fi prepared by ACLJS in this work showed better performance than other systems in the literature using the same Platinum/Vulcan electrocatalyst despite having significantly lower catalyst loading.[24,30–32] The comparison of this work to the literature will be expanded in the Comparison of ACLJS spraying to other PEMFC electrode fabrication methods section.

The effect of fuel and oxidant relative humidity on the performance of the Fiber type breakup CCMs.—Relative humidity (RH) has been reported to have a significant impact on PEMFC performance and oxygen reduction kinetics.[33–36] The sensitivity of CCM-Fi to inlet gas relative humidity was investigated. The cell was tested under H_2/O_2 flow with stoichiometry of 2 at 150 $kPa_{(absolute)}$. As the RH was reduced from 81% to 53%, the cell performance showed a volcano-type behavior. This observation results from a tradeoff: high relative humidity leads to CL flooding, while low relative humidity brings about membrane dry out that increases ohmic resistance. CCM-Fi attained the highest performance at 60% RH for the both anode and cathode, implying the cell prefers a low humidification operating condition because of its high performance and internal water production and back diffusion. Low RH operation is ideal for portable power applications, including transportation, due to the obviation of saturating the reactant gases.[37] It was found that the performance of CCMs prepared by the air-assisted cylindrical jet spray system was more sensitive to fuel RH (Figure 7a) than to oxidant RH when the cell was operated at high current density (Figure 7b), which was logical from a water management point of view. A significant amount of water is dragged from the anode to the cathode, in addition to being produced at the cathode, meaning that there is always significant water at the cathode. Thus, the anode and membrane are prone to drying out when the cell is operated at high current densities. However, the oxygen humidification did have an impact on the electrode kinetics, which is shown in the inset of Figure 7, probably due to a direct influence on proton and water activity at the cathode side.[35] The cell performance improvement at low relative humidity might also be a result of the low loading, as thin catalyst layers have an increased tendency to flood.

Comparison of ACLJS spraying to other PEMFC electrode fabrication methods.—Though many techniques have been reported by various groups for the fabrication of PEMFC electrodes, there still does not exist a standard technique that is commonly used (even at the lab scale) to produce CCMs or gas diffusion electrodes. Because a common technique is lacking, it is very difficult to compare results across laboratories throughout the literature. What is needed is a low cost method that is relatively simple to operate that can produce high-performing CCMs and/or GDEs. Based on the high performance of the CCMs produced in this work, the understanding of the influence of spray parameters on CCM structure reported here, and the low cost of the lab scale-ACLJS (~$4000 USD, supporting information), the ACLJS makes a compelling case to become such a standard CCM fabrication approach.

A comparison of the CCM-Fi ACLJS electrodes to electrodes recently produced by various other methods is shown in Table I. In general, the ACLJS method offers excellent performance in terms of both current density at 0.7 V and peak power density, with 1.9 A/cm^2

Table I. Comparison of currently representative low Pt loading PEMFC electrodes fabrication methods

Technique	Pt catalyst loading (mg/cm^2)		GDL type	Membrane type	Current density (A/cm^2) at 0.7 V	Peak power density (W/cm^2)	Total Peak Power per Pt loading (W/mg$_{Pt}$)	Operating condition			
	Cathode	Anode						Pressure (Kpa)	T_{cell}(°C)	RH (Ca/An)	Gas type (An/Ca)
ACLJS	0.3	0.3	SGL 25BC	Nafion 212	1.9 (O_2)/0.7 (Air)	1.33 (O_2)/0.6 (Air)	4.43 (O_2)/2.0 (Air)	150/150	80	75%/81%	H_2/O_2; H_2/Air
Spraying[41]	0.232	0.116	SGL 24BC	Nafion 212	0.4 (Air)	0.5	2.87	Ambient	65	100%/100%	H_2/Air
RSDT[38]	0.07	0.07	SGL 25BC	Nafion 211	0.6 (O_2)/0.25(Air)	0.9 (O_2)/0.45(Air)	12.8 (O_2)/6.4 (Air)	Ambient	80	100%/100%	H_2/O_2; H_2/Air
Decal transfer[42]	0.42	0.42	SGL 10BC	NRE-212	0.45(Air)	0.4	0.95	Ambient	65	95%/95%	H_2/Air
Ultrasonic-spray[43]	0.4	0.4	SGL 24BC	Nafion 212	0.73 (O_2)	0.695	1.74	200/200	70	50%/50%	H_2/O_2
Screen Printing[44]	0.3	0.3	Toray carbon paper	Nafion 212	0.5 (O_2)	0.66	2.2	Ambient	65	100%/100%	H_2/O_2
Inkjet Printing[45]	1	1	———	Nafion 117	0.1 (O_2)	0.113	0.113	———	40	———	H_2/O_2
CVD[46]	0.2	0.2	———	Nafion 212	0.7 (O_2)	0.86	4.3	97/97	75	———	H_2/O_2
Electrospraying[39]	0.01	0.01	Toray carbon paper	Nafion 212	0.5 (O_2)	0.709	70.9	440/440	70	Dry	H_2/O_2
Spraying[47]	0.4	0.2	SGL 10BC	Nafion 212	0.5 (O_2)	0.899	3.0	Ambient	80	100%/100%	H_2/O_2
DMD[40]	0.102	0.102	SGL 24BC	Nafion D 2020	1.4 (O_2)	2.93	28.7	300/300	80	75%/75%	H_2/O_2

and 1.33 W/cm^2, respectively. The ACLJS method also shows very high performance with regard to peak power when normalized to the Pt mass (4.43 W/mg$_{Pt}$), though lower than reactive spray deposition technology (RSDT), direct membrane deposition (DMD) method and electrospray method.[38–40] However, it should be noted that RSDT is very expensive to implement on the laboratory scale (~$150,000 USD) and has a significant number of adjustable parameters, which may limit its widespread application in a university or R&D setting, though it remains promising at larger scales. By comparison, the ACLJS is a fairly economic process, where only a small amount of electricity and nitrogen gas are consumed. DMD has the potential issue of high gas crossover rates; in order to avoid that problem, an extra subgasket has to be used, which reduces the active cell area. Electrospraying has shown a very high mass-normalized performance at low Pt loading (around 70 W/mg$_{Pt}$); however, the peak power density was low - only 0.7 W/cm^2 for 5 cm^2 cell active area. Additionally, the electrospraying rate was only 0.2 ml h^{-1}, which may limit the active area size that can be created as well as possible ink phase separation from catalyst settling during deposition. Another comparable technique in terms of performance is chemical vapor deposition (CVD) with a Pt normalized peak power density of 4.3 W/mg$_{Pt}$. However, the main problem for the CVD technique is low throughput combined with high cost. Also, the CVD-derived electrodes had a lower areal performance than the ACLJS. It should also be noted that the CVD technique used carbon nanotube as the catalyst support and the cell active area was only 5 cm^2. Overall, Table I shows that the ACLJS is a promising and practical technique to prepare high performing MEAs at least in a university or R&D lab setting. The possible application of the ACLJS at commercial scales is interesting, but has not yet been investigated; therefore, the other MEA fabrication methods discussed here cannot be dismissed from a manufacturing perspective where at least some of their drawbacks at small scales may be more or less overcame at larger scales.

Conclusions

A low cost CCM preparation method – air-assisted cylindrical liquid jet spray system – was developed and the CCMs prepared by the ACLJS method showed high performance during PEMFC testing. Mercury intrusion porosimetry showed that the total pore volume of the CCM varied greatly at different spraying conditions. When tested by EIS and PEMFC polarization, the CCM with highest total pore volume had the best mass transport and least charge transfer resistance as well as a current density greater than 1900 mA/cm^2 at 0.7 V under H_2/O_2 flows and 700 mA/cm^2 under H_2/Air at 1.5 bar$_{(absolute)}$ pressure and 60% gas RH, and 80°C cell temperature. Based on the CCM-Fi prepared by the ACLJS method, it is also found that the fuel relative humidity had a greater impact on PEMFC performance than oxidant relative humidity, most likely due to water production on the cathode side.

Acknowledgments

This work was supported by the U. S. Department of Energy (DOE) award number DE-SC0010531. The author acknowledges the Center for Clean Energy Engineering at the University of Connecticut for free use of the physical characterization equipment.

References

1. R. F. Service, *Science (80-.).*, **296**, 1222 (2002).
2. S. Cleghorn, *Int. J. Hydrogen Energy*, **22**, 1137 (1997).
3. H. Zhang and P. K. Shen, *Chem. Rev.*, **112**, 2780 (2012).
4. M. S. Wilson, *J. Electrochem. Soc.*, **139**, L28 (1992).
5. C. Chen et al., *Science*, **343**, 1339 (2014).
6. M. S. Saha, D. K. Paul, B. A. Peppley, and K. Karan, *Electrochem. commun.*, **12**, 410 (2010).
7. İ. Fırtına, S. Güner, and A. Albostan, *Int. J. Energy Res.*, **35**, 146 (2011).
8. J. Cao et al., *Int. J. Hydrogen Energy*, **35**, 4622 (2010).
9. C. S. Kong, D.-Y. Kim, H.-K. Lee, Y.-G. Shul, and T.-H. Lee, *J. Power Sources*, **108**, 185 (2002).
10. H. Yu et al., *J. Electrochem. Soc.*, **161**, F622 (2014).
11. Y. Song, J. M. Fenton, H. R. Kunz, L. J. Bonville, and M. V. Williams, *J. Electrochem. Soc.*, **152**, A539 (2005).
12. J. W. Ihm, H. Ryu, J. S. Bae, W. K. Choo, and D. K. Choi, *J. Mater. Sci.*, **39**, 4647 (2004).
13. K. Bolwin, E. Giilzow, D. Bevers, and W. Schnumberger, *Solid State Ionics*, **2738**, 324 (1995).
14. A. P. Saab, F. H. Garzon, and T. A. Zawodzinski, *J. Electrochem. Soc.*, **149**, A1541 (2002).
15. J. Zhang, G. Yin, Z. Wang, and Y. Shao, *J. Power Sources*, **160**, 1035 (2006).
16. Y. F. Zheng, R. F. Wu, W. Shi, Z. Q. Guan, and J. S. Yu, *Sol. Energy Mater. Sol. Cells*, **111**, 200 (2013).
17. C. Dumouchel, "On the experimental investigation on primary atomization of liquid streams," *Experiments in Fluids*, **45**, 371 (2008).
18. E. Villermaux, P. Marmottant, and J. Duplat, *Phys. Rev. Lett.*, **92**, 74501 (2004).
19. J. C. Lasheras, E. Villermaux, and E. J. Hopfinger, *J. Fluid Mech.*, **357**, 351 (1998).
20. M. S. Saha, D. Paul, S. Malevich, B. Peppley, and K. Karan, "Preparation of Ultra-Thin Catalyst Layers by Piezo-electric Printer for PEMFCs Applications, " *ECS Transactions*, **25**, 2049 (2009).
21. J. Ihonen, F. Jaouen, G. Lindbergh, A. Lundblad, and G. Sundholm, *J. Electrochem. Soc.*, **149**, A448 (2002).
22. M. Eikerling, *J. Electrochem. Soc.*, **153**, E58 (2006).
23. C.-Y. Jung, W.-J. Kim, and S.-C. Yi, *Int. J. Hydrogen Energy*, **37**, 18446 (2012).
24. D. S. Hwang, C. H. Park, S. C. Yi, and Y. M. Lee, *Int. J. Hydrogen Energy*, **36**, 9876 (2011).
25. X. Yuan, H. Wang, J. Colinsun, and J. Zhang, *Int. J. Hydrogen Energy*, **32**, 4365 (2007).
26. Z. Xie and S. Holdcroft, *J. Electroanal. Chem.*, **568**, 247 (2004).
27. X. Yuan et al., *J. Power Sources*, **161**, 920 (2006).
28. X. YAN et al., *Int. J. Hydrogen Energy*, **32**, 4358 (2007).
29. F. Liu et al., *J. Power Sources*, **124**, 81 (2003).
30. K. H. Kim et al., *Int. J. Hydrogen Energy*, **35**, 2119 (2010).
31. S. Mu and M. Tian, *Electrochim. Acta*, **60**, 437 (2012).
32. A. D. Taylor, E. Y. Kim, V. P. Humes, J. Kizuka, and L. T. Thompson, *J. Power Sources*, **171**, 101 (2007).
33. Q. fei Jian, G. qing Ma, and X. liang Qiu, *Renew. Energy*, **62**, 129 (2014).
34. J. H. Kim et al., *J. Electrochem. Soc.*, **157**, B633 (2010).
35. K. C. Neyerlin, H. a. Gasteiger, C. K. Mittelsteadt, J. Jorne, and W. Gu, *J. Electrochem. Soc.*, **152**, A1073 (2005).
36. M. Ouattara-Brigaudet, S. Berthon-Fabry, C. Beauger, and P. Achard, *Int. J. Hydrogen Energy*, **39**, 1420 (2014).
37. V. Ramani, H. R. Kunz, and J. M. Fenton, *J. Memb. Sci.*, **232**, 31 (2004).
38. H. Yu, J. M. Roller, W. E. Mustain, and R. Maric, *J. Power Sources*, **283**, 84 (2015).
39. S. Martin and J. L. Castillo, *J. Power Sources*, **229**, 179 (2017).
40. M. Breitwieser et al., *Electrochem. commun.*, **60**, 168 (2015).
41. T. Huang, H. Shen, T. Jao, F. Weng, and A. Su, "Ultra-low pt loading for proton exchange membrane fuel cells by catalyst coating technique with ultrasonic spray coating machine," *International Journal of Hydrogen Energy*, **37**(18), 13872 (2012).
42. S. Jeon et al., *Int. J. Hydrogen Energy*, **35**, 9678 (2010).
43. B. Millington, V. Whipple, and B. G. Pollet, *J. Power Sources*, **196**, 8500 (2012).
44. W. Wang, S. Chen, J. Li, and W. Wang, *Int. J. Hydrogen Energy*, **40**, 4649 (2015).
45. Z. Wang and Y. Nagao, *Electrochim. Acta*, **129**, 343 (2014).
46. Y. Yuan et al., *J. Power Sources*, **196**, 6160 (2011).
47. T. Truc, T. L. Yu, and H. Lin, *J. Power Sources*, **225**, 293 (2013).